J|A|C|S
ARTICLES

Published on Web 05/14/2008

Triplet Pathways in Diarylethene Photochromism: Photophysical and Computational Study of Dyads Containing Ruthenium(II) Polypyridine and 1,2-Bis(2-methylbenzothiophene-3-yl)maleimide Units

Maria Teresa Indelli,*,† Stefano Carli,† Marco Ghirotti,† Claudio Chiorboli,‡,§ Marcella Ravaglia,*,† Marco Garavelli,|| and Franco Scandola*,†,‡

Dipartimento di Chimica, Università di Ferrara, 44100 Ferrara, Italy, INSTM, Sezione di Ferrara, 44100 Ferrara, Italy, ISOF-CNR, Sezione di Ferrara, 44100 Ferrara, Italy, and Dipartimento di Chimica "G. Ciamician", Via Selmi 2, 40126 Bologna, Italy

Received January 21, 2008; E-mail: snf@unife.it

Abstract: A 1,2-bis(2-methylbenzothiophene-3-yl)maleimide model (**DAE**) and two dyads in which this photochromic unit is coupled, via a direct nitrogen−carbon bond (**Ru-DAE**) or through an intervening methylene group (**Ru-CH_2-DAE**), to a ruthenium polypyridine chromophore have been synthesized. The photochemistry and photophysics of these systems have been thoroughly characterized in acetonitrile by a combination of stationary and time-resolved (nano- and femtosecond) spectroscopic methods. The diarylethene model **DAE** undergoes photocyclization by excitation at 448 nm, with 35% photoconversion at stationary state. The quantum yield increases from 0.22 to 0.33 upon deaeration. Photochemical cycloreversion (quantum yield, 0.51) can be carried out to completion upon excitation at $\lambda > 500$ nm. Photocyclization takes place both from the excited singlet state (S_1), as an ultrafast (ca. 0.5 ps) process, and from the triplet state (T_1) in the microsecond time scale. In **Ru-DAE** and **Ru-CH_2-DAE** dyads, efficient photocyclization following light absorption by the ruthenium chromophore occurs with oxygen-sensitive quantum yield (0.44 and 0.22, in deaerated and aerated solution, respectively). The photoconversion efficiency is almost unitary (90%), much higher than for the photochromic **DAE** alone. Efficient quenching of both Ru-based MLCT phosphorescence and **DAE** fluorescence is observed. A complete kinetic characterization has been obtained by ps−ns time-resolved spectroscopy. Besides prompt photocyclization (0.5 ps), fast singlet energy transfer takes place from the excited diarylethene to the Ru(II) chromophore (30 ps in **Ru-DAE**, 150 ps in **Ru-CH_2-DAE**). In the Ru(II) chromophore, prompt intersystem crossing to the MLCT triplet state is followed by triplet energy transfer to the diarylethene (1.5 ns in **Ru-DAE**, 40 ns in **Ru-CH_2-DAE**). The triplet state of the diarylethene moiety undergoes cyclization in a microsecond time scale. The experimental results are complemented with a combined *ab initio* and DFT computational study whereby the potential energy surfaces (PES) for ground state (S_0) and lowest triplet state (T_1) of the diarylethene are investigated along the reaction coordinate for photocyclization/cycloreversion. At the DFT level of theory, the transition-state structures on S_0 and T_1 are similar and lean, along the reaction coordinate, toward the closed-ring form. At the transition-state geometry, the S_0 and T_1 PES are almost degenerate. Whereas on S_0 a large barrier (ca. 45 kcal mol^{-1}) separates the open- and closed-ring minima, on T_1 the barriers to isomerization are modest, cyclization barrier (ca. 8 kcal mol^{-1}) being smaller than cycloreversion barrier (ca. 14 kcal mol^{-1}). These features account for the efficient sensitized photocyclization and inefficient sensitized cycloreversion observed with **Ru-DAE**. Triplet cyclization is viewed as a nonadiabatic process originating on T_1 at open-ring geometry, proceeding via intersystem crossing at transition-state geometry, and completing on S_0 at closed-ring geometry. A computational study of the prototypical model 1,2-bis(3-thienyl)ethene is used to benchmark DFT results against *ab initio* CASSCF//CASPT2 results and to demonstrate the generality of the main topological features of the S_0 and T_1 PES obtained for **DAE**. Altogether, the results provide strong experimental evidence and theoretical rationale for the triplet pathway in the photocyclization of photochromic diarylethenes.

Introduction

Photochromism is of great interest in a variety of practical fields, including the development of optoelectronic devices, memories, and switches.[1–3] Diarylethenes with heterocyclic aryl groups are a particularly interesting class of photochromic systems undergoing very efficient, thermally irreversible, fatigue-resistant photocyclization-cycloreversion reactions (e.g., Figure 1). Extensive work, particularly by Irie and co-workers,[4–10] has addressed several aspects of this remarkable class of

† Università di Ferrara.
‡ INSTM, Sezione di Ferrara.
§ ISOF-CNR, Sezione di Ferrara.
|| G. Ciamician.

(1) Irie, M. *Chem. Rev.* **2000**, *100*, 1683–1890, Special issue on "Photochromism: memories and switches"
(2) Feringa, B. L. Ed. *Molecular Switches*; Wiley-VCH: Weinheim, 2001.

10.1021/ja711173z CCC: $40.75

compounds, such as synthesis, thermal stability, quantum yields, fatigue-resistance, conformational effects, gating (for nondestructive readout), optical memory applications, single-molecule photochromism, and photomechanical effects. A variety of experimental techniques (e.g., fast and ultrafast spectroscopy,[11–20] waveguide spectroscopy,[21–23] near-field scanning optical microscopy,[24–27] transmission electron microscopy,[28] two-dimensional FTIR spectroscopy,[29,30] Raman spectroscopy,[31,32] and single-molecule spectroscopy[5,9,33]), as well as theoretical methods (*ab initio* correlated methods,[34,35] semiempirical methods,[17,36–38] and density functional methods[31,39,40]) have been applied to photochromic diarylethenes. The ultrafast studies show that the open and closed forms undergo cyclization and cycloreversion, respectively, in less than a few picoseconds. This is in agreement with the results of the theoretical investigations, which show the presence of almost barrierless pathways connecting the lowest excited singlet state to the ground-state of the isomerized form, via conical intersections.[34] Developments in the field of diarylethene photochromic switches have been reviewed.[4,8,41–43]

Figure 1. Schematic representation of photocyclization/cycloreversion in a diarylethene based on thiophene aryl groups. The central double bond is included in a cyclic structure (usually penta-atomic, schematized by the circular fragment) that prevents cis−trans photoisomerization.

In the context of supramolecular photochemistry,[44] we have been studying for some time intramolecular photoinduced energy and electron transfer processes in covalently linked donor−acceptor systems (dyads, triads, etc.) involving metal complexes.[45–47] As an extension of that work, we set up to explore the possibility of including photochromic molecular components in the design of our supramolecular systems. Reasons of interest can be summarized as follows: (i) the decoupling of the light-absorbing and color-switching functions, with potentially enhanced tuning capability; (ii) the possibility to obtain sensitized photochromism, with different quantum yields and photostationary states with respect to direct excitation; (iii) the possibility to use a photochromic component to switch on/off the excited-state properties (e.g., emission) of a sensitizer unit; (iv) the possibility to access by sensitization unusual triplet pathways for diarylethene photochromism.

This last aspect is of particular interest to the present work. As a matter of fact, the photochemical processes of diarylethenes are usually interpreted[48] in the general theoretical framework of [6]electrocyclic reactions, whereby conrotatory ring closure/opening, forbidden in the ground state, is allowed in excited singlet states. Triplet reaction pathways, on the other hand, are

(3) Dürr, H., Bouas-Laurent, H., Eds. *Photochromism: Molecules and Systems*, Elsevier: Amsterdam, 2003.
(4) Irie, M. *Chem. Rev.* **2000**, *100*, 1685–1716.
(5) Irie, M.; Fukaminato, T.; Sasaki, T.; Tamai, N.; Kawai, T. *Nature* **2002**, *420*, 759–760.
(6) Higashiguchi, K.; Matsuda, K.; Irie, M. *Angew. Chem., Int. Ed.* **2003**, *42*, 3537–3540.
(7) Matsuda, K.; Irie, M. *J. Photochem. Photobiol., C* **2004**, *5*, 169–182.
(8) Higashiguchi, K.; Matsuda, K.; Tanifuji, N.; Irie, M. *J. Am. Chem. Soc.* **2005**, *127*, 8922–8923.
(9) Fukaminato, T.; Umemoto, T.; Iwata, Y.; Yokojima, S.; Yoneyama, M.; Nakamura, S.; Irie, M. *J. Am. Chem. Soc.* **2007**, *129*, 5932–5938.
(10) Kobatake, S.; Takami, S.; Muto, H.; Ishikawa, T.; Irie, M. *Nature* **2007**, *446*, 778–781.
(11) Miyasaka, H.; Araki, S.; Tabata, A.; Nobuto, T.; Mataga, N.; Irie, M. *Chem. Phys. Lett.* **1994**, *230*, 249–254.
(12) Miyasaka, H.; Nobuto, T.; Itaya, A.; Tamai, N.; Irie, M. *Chem. Phys. Lett.* **1997**, *269*, 281–285.
(13) Owrutsky, J. C.; Nelson, H. H.; Baronavski, A. P.; Kim, O. K.; Tsivgoulis, G. M.; Gilat, S. L.; Lehn, J. M. *Chem. Phys. Lett.* **1998**, *293*, 555–563.
(14) Sasaki, K.; Nagamura, T. *J. Appl. Phys.* **1998**, *83*, 2894–2900.
(15) Ern, J.; Bens, A. T.; Martin, H. D.; Mukamel, S.; Schmid, D.; Tretiak, S.; Tsiper, E.; Kryschi, C. *Chem. Phys.* **1999**, *246*, 115–125.
(16) Tamai, N.; Miyasaka, H. *Chem. Rev.* **2000**, *100*, 1875–1890.
(17) Ern, J.; Bens, A. T.; Martin, H. D.; Mukamel, S.; Tretiak, S.; Tsyganenko, K.; Kuldova, K.; Trommsdorff, H. P.; Kryschi, C. *J. Phys. Chem. A* **2001**, *105*, 1741–1749.
(18) Bertarelli, C.; Gallazzi, M. C.; Stellacci, F.; Zerbi, G.; Stagira, S.; Nisoli, M.; De Silvestri, S. *Chem. Phys. Lett.* **2002**, *359*, 278–282.
(19) Hania, P. R.; Telesca, R.; Lucas, L. N.; Pugzlys, A.; van Esch, J.; Feringa, B. L.; Snijders, J. G.; Duppen, K. *J. Phys. Chem. A* **2002**, *106*, 8498–8507.
(20) Murakami, M.; Miyasaka, H.; Okada, T.; Kobatake, S.; Irie, M. *J. Am. Chem. Soc.* **2004**, *126*, 14764–14772.
(21) Cattaneo, S.; Lecomte, S.; Bosshard, C.; Montemezzani, G.; Gunter, P.; Livingston, R. C.; Diederich, F. *J. Opt. Soc. Am. B: Opt. Phys.* **2002**, *19*, 2032–2038.
(22) Ishitobi, H.; Mizuhara, Y.; Sekkat, Z.; Kawata, S. *Jpn. J. Appl. Phys., Part 1* **2004**, *43*, 814–816.
(23) Kang, J. W.; Kim, J. J.; Kim, E. *Appl. Phys. Lett.* **2002**, *80*, 1710–1712.
(24) Horie, K.; Murase, S.; Takahashi, S.; Teramoto, M.; Furukawa, H. *Macromol. Symp.* **2003**, *195*, 201–208.
(25) Kim, J.; Song, K. B.; Park, K. H.; Lee, H. W.; Kim, E. *Jpn. J. Appl. Phys., Part 1* **2002**, *41*, 5222–5225.
(26) Lee, H. W.; Kim, Y. M.; Jeon, D. J.; Kim, E.; Kim, J.; Park, K. *Opt. Mater.* **2003**, *21*, 289–293.
(27) Yamamoto, N.; Mizokuro, T.; Mochizuki, H.; Horiuchi, S.; Hayakawa, T.; Hiraga, T. *J. Microsc.* **2004**, *213*, 135–139.
(28) Han, M.; Lee, E.; Kim, E. *Opt. Mater.* **2003**, *21*, 579–583.
(29) Wang, Q.; Sun, S. Q.; Guo, H. B.; Zhou, Q.; Noda, I.; Hua, X. Y. *Vib. Spectrosc.* **2003**, *31*, 257–263.
(30) Wang, Q.; Sun, S. Q.; Guo, H. B.; Zhou, Q.; Hu, X. Y. *Spectrosc. Spectral Anal.* **2003**, *23*, 859–862.
(31) Okabe, C.; Tanaka, N.; Fukaminato, T.; Kawai, T.; Irie, M.; Nibu, Y.; Shimada, H.; Goldberg, A.; Nakamura, S.; Sekiya, H. *Chem. Phys. Lett.* **2002**, *357*, 113–118.
(32) Okabe, C.; Nakabayashi, T.; Nishi, N.; Fukaminato, T.; Kawai, T.; Irie, M.; Sekiya, H. *J. Phys. Chem. A* **2003**, *107*, 5384–5390.
(33) Fukaminato, T.; Sasaki, T.; Kawai, T.; Tamai, N.; Irie, M. *J. Am. Chem. Soc.* **2004**, *126*, 14843–14849.
(34) Boggio-Pasqua, M.; Ravaglia, M.; Bearpark, M. J.; Garavelli, M.; Robb, M. A. *J. Phys. Chem. A* **2003**, *107*, 11139–11152.
(35) Guillaumont, D.; Kobayashi, T.; Kanda, K.; Miyasaka, H.; Uchida, K.; Kobatake, S.; Shibata, K.; Nakamura, S.; Irie, M. *J. Phys. Chem. A* **2002**, *106*, 7222–7227.
(36) Delaire, J. A.; Fanton-Maltey, I.; Chauvin, J.; Nakatani, K.; Irie, M. *Mol. Cryst. Liq. Cryst.* **2000**, *345*, 557–562.
(37) Cho, H. G.; Cheong, B. S. *Bull. Korean Chem. Soc.* **1998**, *19*, 308–313.
(38) Kojima, M.; Ishida, A.; Takamuku, S. *Bull. Chem. Soc. Jpn.* **1998**, *71*, 2211–2220.
(39) Majumdar, D.; Lee, H. M.; Kim, J.; Kim, K. S.; Mhin, B. J. *J. Chem. Phys.* **1999**, *111*, 5866–5872.
(40) Tanaka, N.; Okabe, C.; Sakota, K.; Fukaminato, T.; Kawai, T.; Irie, M.; Goldberg, A.; Nakamura, S.; Sekiya, H. *J. Mol. Struct.* **2002**, *616*, 113–118.
(41) Myles, A. J.; Branda, N. R. *Adv. Funct. Mater.* **2002**, *12*, 167–173.
(42) Tian, H.; Yang, S. J. *Chem. Soc. Rev.* **2004**, *33*, 85–97.
(43) Tian, H.; Wang, S. *Chem. Commun.* **2007**, 781–792.
(44) Balzani, V.; Scandola, F. *Supramolecular Photochemistry*; Harwood: Chichester, 1991.
(45) Scandola, F.; Chiorboli, C.; Indelli, M. T.; Rampi, M. A. In *Electron Transfer in Chemistry*; Balzani, V. Ed.; Wiley-VCH: Weinheim, 2001; Vol. III, Chapter 2.3, p 337.
(46) Chiorboli, C.; Indelli, M. T.; Scandola, F. *Top. Curr. Chem.* **2005**, *257*, 63–102.
(47) Scandola, F.; Chiorboli, C.; Prodi, A.; Iengo, E.; Alessio, E. *Coord. Chem. Rev.* **2006**, *250*, 1471–1496.
(48) Nakamura, S.; Irie, M. *J. Org. Chem.* **1988**, *53*, 6136–6138.

not usually considered, as they would either produce high-energy triplet products or need a mechanism for efficient intersystem crossing to ground state. Recently, however, a number of systems where a diarylethene photochromic unit is coupled to a transition metal complex moiety have been reported.[49–55] In particular, triplet sensitization of diarylethene photocyclization has been demonstrated by De Cola and co-workers[54,55] in a binuclear Ru(II) complex with a photochromic diarylethene bridging ligand unit and by Yam and co-workers[51–53] in Re(I) metal complexes with a bis-thienyl substituted phenanthroline ligand.

We present here the results of a detailed photochemical/photophysical study of dyads **Ru-DAE** and **Ru-CH$_2$-DAE**, where a standard ruthenium polypyridine chromophore is covalently coupled to a 1,2-bis(2-methylbenzothiophene-3-yl)maleimide photochromic moiety at the imide position, either directly (**Ru-DAE**) or through a methylene spacer (**Ru-CH$_2$-DAE**). This particular type of diarylethene unit, of the 1,2-diarylmaleimide type,[56,57] was chosen for synthetic reasons (ease of functionalization at the imide nitrogen) and on the basis of excited-state energy considerations (*vide infra*). For comparison purposes, the model systems **DAE**[58] and **Ru** have also been investigated. The dyads are investigated by standard photochemical and photophysical techniques, as well as with nanosecond and femtosecond time-resolved spectroscopy, with the aim to provide a detailed mechanistic and kinetic characterization.

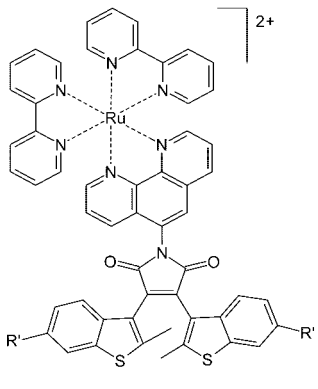

Ru-DAE

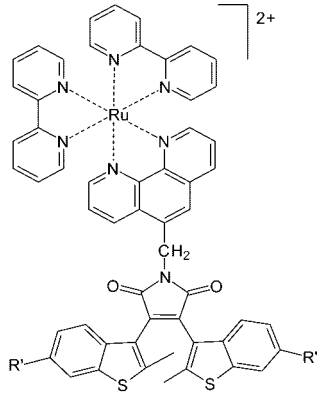

Ru-CH$_2$-DAE

To rationalize the observed triplet reactivity in this class of compounds, we have also carried out a computational study on model systems of the diarylethene unit. For **DAE**,[58] the triplet (T_1) and ground-state (S_0) potential energy surfaces (PES) have been investigated in detail by DFT techniques. The effective electronic decoupling of the diarylethene moiety from the complex moiety in the dyads has been checked by DFT calculations on **phen-DAE**. A combined *ab initio* and DFT study of the model system 1,2-bis(3-thienyl)ethene (**mod-DAE**) has also been performed to benchmark DFT against CASSCF//CASPT2 results and to demonstrate the generality of the main topological features of the S_0 and T_1 PES. The computational study yields a working model for the interpretation of the triplet reactivity of diarylethenes.

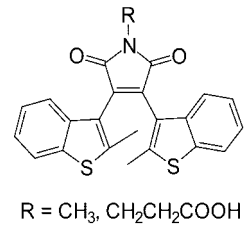

R = CH$_3$, CH$_2$CH$_2$COOH

DAE

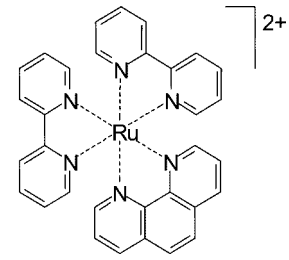

Ru

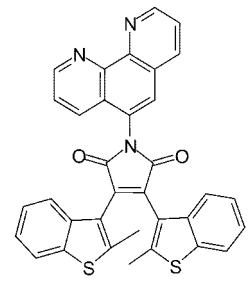

phen-DAE

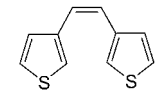

mod-DAE

Experimental and Computational Methods

Materials. All reagents were purchased from Sigma-Aldrich and used as received. For photophysical measurements spectrograde organic solvents were used without further purification.

Reactions were monitored on TLC plates (Fluka silica gel TLC-PET foils UV_{254nm}), and compounds were detected with UV/vis lamp and with a $KMnO_{4\ aq}$ 2%. All compounds were purified by flash chromatography on silica gel (40−63 μ, 230−400 mesh). 5-Amino-[1,10] phenanthroline,[59] 2-methyl-benzo[b]thiophene,[60] 5-cyano-[1,10]-phenanthroline,[61] $Ru(bpy)_2Cl_2$,[62] and $[Ru(bpy)_2$-phen$]$ $(PF_6)_2$[63] were prepared according to literature procedures. The syntheses of **DAE**, **Ru-DAE**, and **Ru-CH$_2$-DAE** are described in detail in the Supporting Information.

Apparatus and Procedures. ^{1}H NMR and ^{13}C NMR spectra were recorded on a Varian Mercury spectrometer (400 MHz). Chemical shifts (δ) are given in ppm, using the residual nondeuterated solvent signal as reference. The coupling constants (J) are given in Hertz. Infrared (IR) spectra were obtained using a FT-IR Nicolet 510P. Electron spray ionization (ESI) mass spectra were measured with a Micromass ZMD2000 spectrometer.

(49) Fernández-Acebes, A.; Lehn, J.-M. *Chem.−Eur. J.* **1999**, *5*, 3285–3292.
(50) Fraysse, S.; Coudret, C.; Launay, J. P. *Eur. J. Inorg. Chem.* **2000**, 1581–1590.
(51) Ko, C.-C.; Kwok, W. M.; Yam, V. W. W.; Phillips, D. L. *Chem.−Eur. J.* **2006**, *12*, 5840–5848.
(52) Yam, V. W. W.; Ko, C.-C.; Zhu, N. *J. Am. Chem. Soc.* **2004**, *126*, 12734–12735.
(53) Lee, P. H. M.; Ko, C.-C.; Zhu, N.; Yam, V. W. W. *J. Am. Chem. Soc.* **2007**, *129*, 6058–6059.
(54) Jukes, R. T. F.; Adamo, V.; Hartl, F.; Belser, P.; De Cola, L. *Inorg. Chem.* **2004**, *43*, 2779–2792.
(55) Jukes, R. T. F.; Adamo, V.; Hartl, F.; Belser, P.; De Cola, L. *Coord. Chem. Rev.* **2005**, *249*, 1327–1335.
(56) Yamaguchi, T.; Uchida, K.; Irie, M. *J. Am. Chem. Soc.* **1997**, *119*, 6066–6071.
(57) Yamaguchi, T.; Matsuo, M.; Irie, M. *Bull. Chem. Soc. Jpn.* **2005**, *78*, 1145–1148.
(58) For practical reasons, the compound with R = CH_2CH_2COOH was used in the experimental study, whereas the model with R = CH_3 was considered in the computational study.
(59) Ellis, C. D.; Margerum, L. D.; Murray, R. W.; Meyer, T. J. *Inorg. Chem.* **1983**, *22*, 1283–1291.
(60) Anderson, W. K.; Lavoie, E. J.; Bottaro, J. C. *J. Chem. Soc., Perkin Trans. 1* **1976**, 1–4.
(61) Shen, Y. B.; Sullivan, B. P. *Inorg. Chem.* **1995**, *34*, 6235–6236.
(62) Sullivan, B. P.; Salmon, D. J.; Meyer, T. J. *Inorg. Chem.* **1978**, *17*, 3334–3341.
(63) Indelli, M. T.; Bignozzi, C. A.; Harriman, A.; Schoonover, J. R.; Scandola, F. *J. Am. Chem. Soc.* **1994**, *116*, 3768–3779.

UV−vis spectra were recorded with a Perkin-Elmer LAMDA40 spectrophotometer. Luminescence spectra were taken on a Spex Fluoromax-2. Emission quantum yields were determined for optically diluted solutions, using $Ru(bpy)_3^{2+}$ as reference. Nanosecond emission lifetimes were measured using a PRA system 3000 Time-correlated Single Photon Counting apparatus equipped with a Norland model 5000 MCA Card, and a Hydrogen discharge pulsing lamp (50 kHz, half-width 2 ns). The decays were analyzed by means of Edinburgh FLA900 software.

Nanosecond transient absorption spectra and lifetimes were measured with an Applied Photophysics laser flash photolysis apparatus, with frequency doubled (532 nm, 330 mJ) or tripled (355 nm, 160 mJ), Surelite Continuum II Nd/YAG laser (half-width 6−8 ns). Photomultiplier (Hamamatsu R928) signals were processed by means of a LeCroy 9360 (600 MHz, 5 Gs/sec) digital oscilloscope.[64] The transient absorption decay measurements were performed in a single shot mode. Transient absorption spectra were obtained from the decays measured at various wavelengths by sampling the absorbance changes at constant delay time. To prevent photocyclization, the probed solution was renewed after each experiment.

Femtosecond time-resolved experiments were performed using a pump−probe spectrometer[65] based on the Spectra-Physics Hurricane Ti:sapphire system as laser source. The pump pulse was generated either by a frequency doubler (400 nm) or with a Spectra Physics 800 OPA (tunable in the range 488−600 nm). The probe−pulse was obtained by continuum generation on a sapphire plate (useful spectral range, 450−800 nm). Effective time resolution ca. 300 fs, temporal chirp over the white-light 450−750 nm range ca. 200 fs, temporal window of the optical delay stage 0−1000 ps. A cuvette with $d = 2$ mm was used. To prevent photocyclization reaction by the laser beam, a stock solution was flowed through the sample cell so that the probed solution was continuously renewed.

Photocyclization quantum yields were determined by monitoring the increasing visible absorbance of the photoproduct upon irradiation (estimated experimental error ± 10%). The photoconversion was kept below 10%. The irradiation source was the Xe lamp (Cermax, 175 W) of the a Perkin-Elmer MPF 44E spectrofluorimeter coupled to a 2nm monochromator. The photon flux was determined before and after each measurement by using Centronic OSD100−7Q calibrated Si photodiode.

All of the experiments and manipulations were performed protecting the solutions against room light.

Computational Methods. Two molecular systems, **phen-DAE** and **DAE**, have been studied at the DFT level of theory. DFT provides an excellent tool for ground state (S_0) and lowest triplet state (T_1) exploration, at a reasonable computational cost, accounting for the correlation energy contribution. All of the geometries have been optimized at the DFT level of theory, using the UB3LYP hybrid functional.[66] Standard basis sets 6-31G and 6-31G* have been used.[67–73] Unrestricted wave functions do not give spin-symmetry adapted wave functions. As a result, a state of given multiplicity might be contaminated by the admixture of high-spin states into the UDFT wave function; thus, it appears appropriate to perform spin projection. Spin-projected energies have been calculated with the approximate spin-correction procedure proposed by Yamaguchi et al.,[74,75] which has been applied by Houk et al.[76] and Garavelli et al.[77] in the study of diradical reaction mechanisms of various organic systems. To evaluate the effect of spin-projection on S_0 energy surface, the UB3LYP/6−31G* singlet ($^1E_{UDFT}$), triplet ($^3E_{UDFT}$), and singlet spin-corrected ($^1E_{SC}$) energies have been computed, assuming that singlet energy contamination arises only from the first higher multiplicity state, T_1 in our system.

$$\Psi_{UDFT} = c_S{}^1\varphi + c_T{}^3\varphi$$

$$^1E_{SC} = {}^1E_{UDFT} + f_{SC}[{}^1E_{UDFT} - {}^3E_{UDFT}]$$

$$f_{SC} = \frac{c_T{}^2}{1 - c_S{}^2} \approx \frac{{}^1\langle S^2\rangle}{{}^3\langle S^2\rangle - {}^1\langle S^2\rangle}$$

It has been suggested[78] that spin projection can degrade the quality of potential energy surfaces calculated by density functional methods. However, in the present case, comparison with CASSCF and PT2 values (see Supporting Information) indicates that spin correction works satisfactorily. No symmetry constraints have been imposed when performing geometry optimizations. Analytical frequency calculations using the same level of theory and computed at the optimized geometry have been used to identify the nature of the stationary point (minima or saddle points). Intrinsic reaction coordinates (IRC) have been calculated from transition structures, to locate minimum-energy paths (MEP) on the potential energy surfaces of interest.

Additional calculations have been performed on **mod-DAE**, using both DFT and an *ab initio* MCSCF (i.e., CASSCF) method. This model system is interesting because of its small size, yet it conserves the essential π system undergoing the electronic rearrangement involved in diarylethene photochromism. Hence, relative to the actual diarylethenes, computational efforts are considerably reduced and allow a more extensive investigation of the potential energy surfaces. CASSCF calculations include in the active space (i.e., the orbitals which can have variable occupancies between 2.0 and 0.0) 10 orbitals among which 10 electrons are distributed. The orbitals chosen are the 10 π, π^* orbitals for the open-ring isomer, whereas for the closed-ring isomer, the 8 π, π^* plus the 2 σ, σ^* orbitals describing the σ bond, the one broken during the cycloreversion photoprocess, are considered. Again, no symmetry constraints have been imposed when performing geometry optimizations. Analytical frequency calculations using the same level of theory and computed at the optimized geometry have been used to identify the nature of the stationary points. The effect of the dynamic electron correlation on the relevant energy profiles and surface topology has been checked using a second order multireference Møller−Plesset perturbation method (CASPT2).[79,80] Standard basis set 6-31G* has been used.

(64) Kleverlaan, C. J.; Indelli, M. T.; Bignozzi, C. A.; Pavanin, L.; Scandola, F.; Hasselman, G. M.; Meyer, G. J. *J. Am. Chem. Soc.* **2000**, *122*, 2840–2849.
(65) Chiorboli, C.; Rodgers, M. A. J.; Scandola, F. *J. Am. Chem. Soc.* **2003**, *125*, 483–491.
(66) Becke, A. D. *J. Chem. Phys.* **1993**, *98*, 1372–1377.
(67) Hehre, W. J.; Stewart, R. F.; Pople, J. A. *J. Chem. Phys.* **1969**, *51*, 2657–2664.
(68) Ditchfield, R.; Hehre, W. J.; Pople, J. A. *J. Chem. Phys.* **1971**, *54*, 724–728.
(69) Hehre, W. J.; Ditchfield, R.; Pople, J. A. *J. Chem. Phys.* **1972**, *56*, 2257–2261.
(70) Hariharan, P. C.; Pople, J. A. *Theor. Chim. Acta* **1973**, *28*, 213–222.
(71) Hariharan, P. C.; Pople, J. A. *Mol. Phys.* **1974**, *27*, 209–214.
(72) Gordon, M. S. *Chem. Phys. Lett.* **1980**, *70*, 343–349.
(73) Petersson, G. A.; Bennett, A.; Tensfeldt, T. G.; Allaham, M. A.; Shirley, W. A.; Mantzaris, J. *J. Chem. Phys.* **1988**, *89*, 2193–2218.
(74) Yamaguchi, K.; Jensen, F.; Dorigo, A.; Houk, K. N. *Chem. Phys. Lett.* **1998**, *149*, 537–542.
(75) Yamanaka, S.; Kawakami, T.; Nagao, H.; Yamaguchi, K. *Chem. Phys. Lett.* **1994**, *231*, 25–33.
(76) Goldstein, E.; Beno, B.; Houk, K. N. *J. Am. Chem. Soc.* **1996**, *118*, 6036–6043.
(77) Garavelli, M.; Bernardi, F.; Olivucci, M.; Robb, M. A. *J. Am. Chem. Soc.* **1998**, *120*, 10210–10222.
(78) Wittbrodt, J. M.; Schlegel, H. B. *J. Chem. Phys.* **1996**, *105*, 6574–6577.
(79) Andersson, K.; Malmqvist, P.-A.; Roos, B. O. *J. Chem. Phys.* **1992**, *96*, 1218–1226.
(80) Andersson, K.; et al. *>MOLCAS*, revision 3.0; University of Lund: Sweden, 1994.

Scheme 1

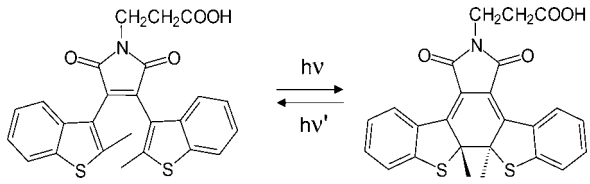

All calculations have been performed with the Gaussian 98 software package.[81]

Results and Discussion

Photochemistry and Photophysics of Diarylethene Models. The photocyclization of **DAE** (Scheme 1) was studied in CH_3CN by irradiation at 448 nm, the most convenient wavelength in terms of reactant/product molar absorptivity ratio (*vide infra*). The starting open form has a maximum at 405 nm, with molar absorptivity of 4250 M^{-1} cm^{-1}.The spectral changes observed upon irradiation (Figure 2) show the development of new absorption bands of the closed form at 361 and 510 nm, reaching a photostationary state at ca. 35% conversion, when the rate of photochemical ring opening equals that of photocyclization. The photolyzed solutions were stable in the dark for days, indicating negligible thermal back reaction. The spectrum of the pure closed form, isolated by thin-layer chromatography (silica, 4:1 cyclohexane:ethylacetate eluent), is also shown in Figure 2 (maxima at 361 and 510 nm, molar absorptivities 10 400 and 5900 M^{-1} cm^{-1}). The quantum yields of photocyclization in air-equilibrated CH_3CN solution was 0.22, and increased to 0.33 upon deaeration.

The photocyclization reaction can be also monitored by ^1H NMR in $CDCl_3$. As commonly found in photochromic diarylethenes,[4–10] the open form of **DAE** has two conformers, a parallel and an antiparallel one, that give rise to distinct methyl signals at 2.1 ppm (parallel) and 2.3 ppm (antiparallel) in $CDCl_3$. From the relative intensity of the two signals, the two conformers are present in a ca. 50% ratio. The photocyclization reaction was monitored following the development of a new methyl signal at 1.98 ppm, characteristic of the closed form. The development of this signal is accompanied by a parallel decrease of both the 2.1 and 2.3 ppm open form signals. As the photocyclization only originates from the antiparallel conformer,[4–10] this indicates that the interconversion of the two conformers of the open form is efficient on the time scale (minutes) of the photochemical experiment.

The photochemical ring opening reaction can be conveniently studied by excitation at $\lambda > 500$ nm, where light absorption by the open form is negligible and the reaction can be easily carried out to completion. The quantum yield is 0.51 in aerated CH_3CN solution. This value justifies the limited photoconversion efficiency obtained upon irradiation at 448 nm. Indeed, considering that 448 nm excitation corresponds to an isosbestic point, the photoconversion efficiency is predicted to be $0.22/(0.22 + 0.51) = 0.3$, in good agreement with the experimental observation (Figure 2).

The open form of **DAE** is emissive, whereas the closed form is not. The fluorescence of the open form in CH_3CN has $\lambda_{max} = 570$ nm and $\Phi = 0.019$. The considerable Stokes shift (165 nm) is consistent with an appreciable charge transfer character

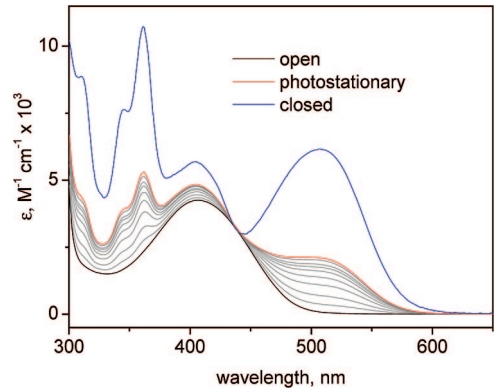

Figure 2. Spectral changes obtained upon continuous photolysis of model compound **DAE** (CH_3CN, 448 nm irradiation), leading from the open form (black line) to a photostationary state (red line). The spectrum of the closed form, obtained by chromatographic separation, is also shown (blue line).

of the excited state.[82] Substantial charge transfer from the benzothiophene moieties to the maleimide unit in the lowest excited-state of this chromophore is indicated by DFT calculations (*vide infra*). The decay of the fluorescence emission is appreciably biexponential, with lifetimes of 2.4 ns (68%) and 1.0 ns (42%). Following the suggestion of Irie and Sayo for related systems,[82] the two components could be assigned to excited-state conformations with different benzothiophene-maleimide torsional angles.

The ultrafast spectroscopy results on **DAE** (CH_3CN, 400-nm excitation) are shown in Figure 3.

The transient spectral changes can be divided in two separate time domains. In the early time scale (0−10 ps), the initial broad transient spectrum, assigned to the singlet excited-state of the open form, evolves with clear formation of a shoulder at ca. 520 nm, indicative of the formation of the closed form. The very short time constant of this process, ca. 0.5 ps, is in line with the general finding that photochemical ring closure of diarylethenes is an ultrafast process.[16] The process is likely to take place via a conical intersection accessible from the Franck−Condon region.[34] In the longer time scale (10−1000 ps), the incipient formation of another transient with a broad absorption in the 600−700 nm range is observed. The time constant for this process, too long to be measured accurately in the time window of the experiment, is of the order of a few nanoseconds. Because this is the time scale of the fluorescence lifetime, it is reasonable to associate the formation of the long-lived transient to the decay of the relaxed singlet state.

The spectrum of the long-lived transient can be better observed by nanosecond flash photolysis (CH_3CN, 355-excitation). It consists of a broad absorption increasing steadily from 400 nm toward the red edge of the spectrum (Figure 4). The transient, formed within the 8 ns laser flash, decays in the microsecond time scale with oxygen-dependent kinetics (10 and 0.30 μs in deaerated and aerated solution, respectively). These features strongly suggest the assignment of the long-lived transient as the triplet state of **DAE**. From a quantitative

(81) Frisch, M. J.; et al. *Gaussian 98*, revision A.7; Gaussian, Inc.: Pittsburgh, PA, 2001.

(82) A similar suggestion was previously made for analogous systems involving maleic anhydride instead of maleimide in: Irie, M.; Sayo, K. *J. Phys. Chem.* **1992**, *96*, 7671–7674.

(83) The comparison between the intensity of the transients is done (i) taking into account the partition of 355 nm excitation light between the two chromophores in Ru-DAE and (ii) measuring at wavelengths ($\lambda > 600$ nm) where the closed isomer photoproduct does not absorb.

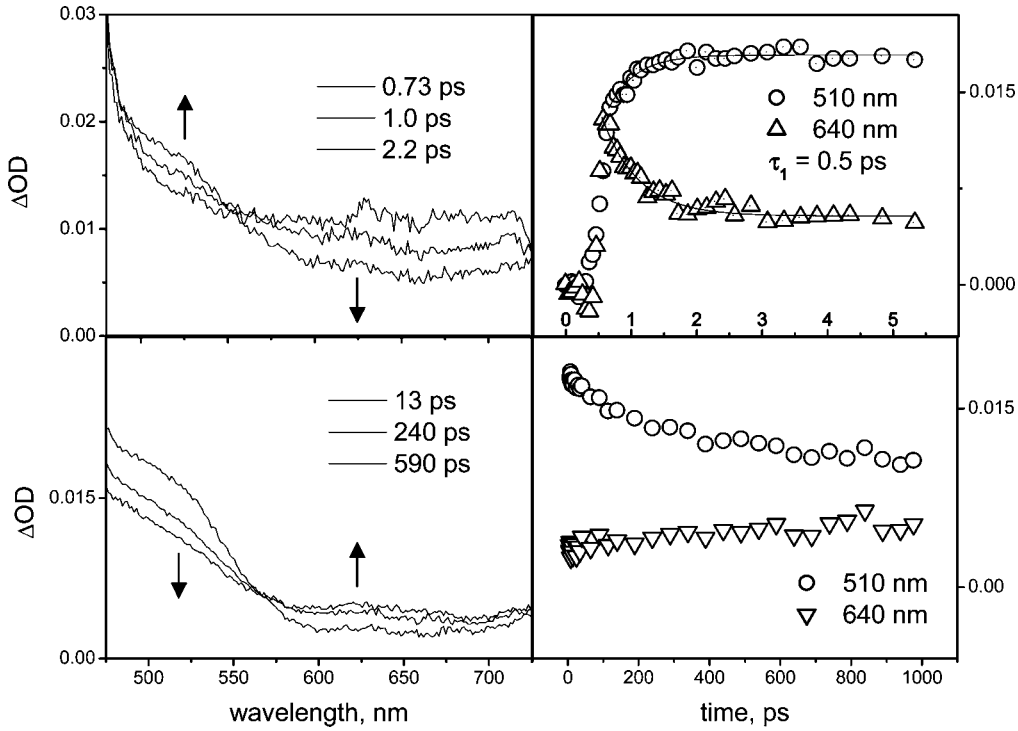

Figure 3. Transient spectra (left) and decay kinetics (right) obtained by femtosecond spectroscopy of model compound **DAE** (CH_3CN, 400 nm excitation).

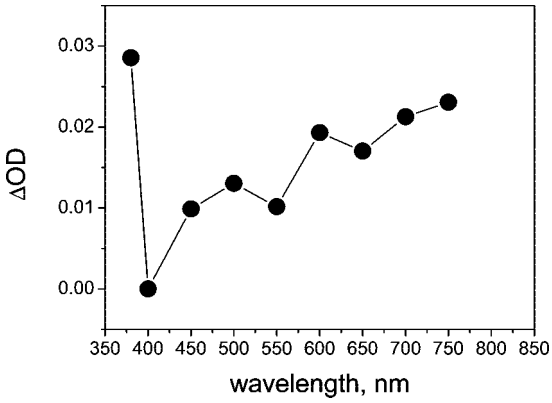

Figure 4. Transient spectrum obtained in laser flash photolysis of model compound **DAE** (CH_3CN, 355 nm excitation, 20 ns time delay).

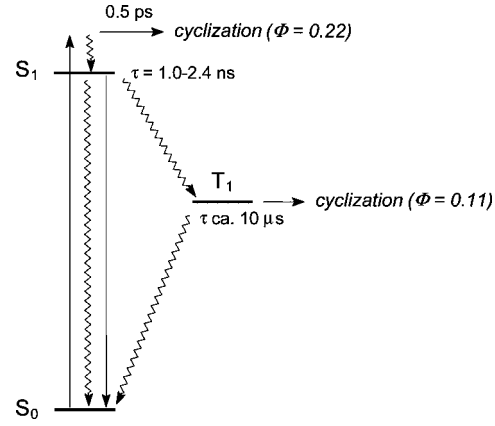

Figure 5. Photocyclization mechanism for model compound **DAE**.

comparison[83] with intramolecular sensitization data obtained with isoabsorptive solutions of **Ru-DAE** (*vide infra*), the efficiency of formation of the triplet state in **DAE** can be estimated as ca. 0.2. A permanent photoproduct, with a spectrum peaking at 510 nm, is left at the end of the transient decay, consistent with formation of the closed isomer. The small increase in the permanent absorption observed in deaerated relative to aerated solution (ca. 20%) represents photoproduct formation from the triplet state. These transient results, together with the oxygen effect on the photoreaction quantum yield (*vide supra*), provide clear evidence for a triplet pathway to photocyclization.

The photocyclization mechanism of **DAE** is summarized in Figure 5. In our measurements, we are not able to discriminate between the behavior of parallel and antiparallel conformers. For instance, the observed fluorescence can in principle arise from (i) the S_1 state of the parallel (unreactive) conformer or (ii) the vibrationally relaxed S_1 state of the antiparallel conformer, reached from the Franck−Condon state in competition with ultrafast reaction.[84] The actual proportion of these two possibilities is unknown. Also, the relative contribution of the two conformers to the observed triplet state formation and reactivity is unknown. Therefore, the mechanism of Figure 5 must be regarded as an overall picture averaging the behavior of the two conformers.

The photochemical and photophysical behavior of **phen-DAE**, which could be considered as an alternative model of the photochromic unit, is practically identical to that of **DAE**. This is not surprising in view of the DFT calculations performed on **phen-DAE**. In the optimized structure, the dihedral angle between the phenanthroline and the maleimide groups is large (ca. 70°), and the π systems of the two fragments, with strongly localized frontier MOs, are efficiently decoupled (for details, see Supporting Information).

(84) Yagi, K.; Soong, C. F.; Irie, M. *J. Org. Chem.* **2001**, *66*, 5419–5423.

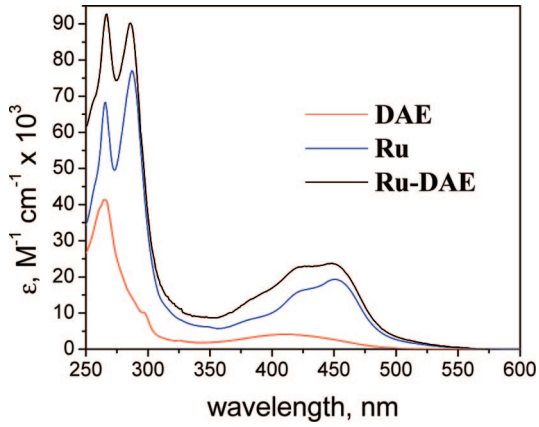

Figure 6. Absorption spectra of dyad **Ru-DAE** (open form) and of the diarylethene **DAE** (open form) and Ru(II) complex **Ru** model molecules.

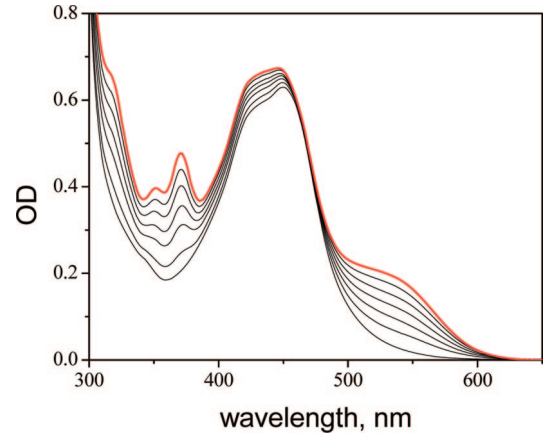

Figure 7. Spectral changes obtained upon continuous photolysis of dyad **Ru-DAE** (air-equilibrated CH_3CN, 470-nm irradiation). The final (red) spectrum corresponds to the photostationary state.

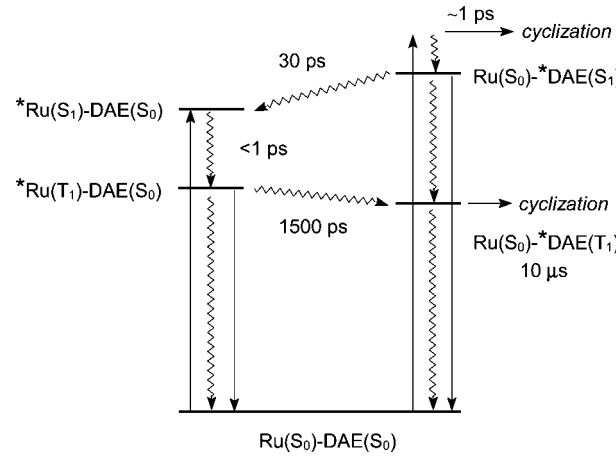

Figure 8. Qualitative energy level diagram and photoclyzation mechanism for dyad **Ru-DAE**.

The significant result of the study of the **DAE** model compound lies in the demonstration that, upon direct excitation, this class of diarylethenes undergo photocyclization not only from the singlet excited-state but also, following intersystem crossing, from the triplet state. Because of the symmetry allowed correlation between the excited singlet state and the ground-state of the isomeric species,[48] diarylethene photochromism is commonly considered to be a singlet state phenomenon. As demonstrated here, however, the role of triplet states should not be disregarded. In fact, if populated with appreciable efficiency, the triplet states, with their long intrinsic lifetimes, can stand relatively slow processes. The computational investigation of the potential energy surfaces of T_1 and S_0 (see below) shows that, in this type of diarylethenes, triplet-state cyclization process is a slightly activated (ca. 8 kcal/mol) process, likely to take place in the microsecond time scale.

Photochemistry and Photophysics of Metal-Complex Diarylethene Dyads. As for the model system **DAE**, the open form of the diarylethene unit in dyad **Ru-DAE** has two conformers distinguishable by ^{1}H NMR, with methyl signals at 2.1 ppm (parallel) and 2.3 ppm (antiparallel) in $CDCl_3$. The two conformers are again present in a ca. 50% ratio, indicating that the presence of the Ru(II) complex unit at the imide position does not alter significantly the conformational equilibrium.[85]

The absorption spectrum of the Ru(II)-complex diarylethene dyad **Ru-DAE** (diarylethene in the open form) is shown in Figure 6, together with those of model systems for the diarylethene (**DAE**) and Ru(II) complex (**Ru**) units. The excellent additivity of the spectra demonstrates the supramolecular nature the system, where the two molecular components are effectively electronically decoupled by the large intercomponent twist angle (for relevant DFT results on **phen-DAE**, see Supporting Information). The visible region of the spectrum is dominated by the metal-to-ligand charge transfer (MLCT) absorption of the Ru(II) complex unit.

The photolysis of **Ru-DAE** was studied in CH_3CN by irradiation with at 470 nm light. At this wavelength, ca. 90% of the absorbed light excites the Ru(II) complex unit. The spectral changes recorded during photolysis are shown in Figure 7. The photoreaction observed is clearly cyclization of the diarylethene unit, with development of the typical bands at 360 and 510 nm of the closed-ring isomer. The photoconversion at photostationary state (estimated using the closed form molar absorptivities of model **DAE**, Figure 2) corresponds to 90%. Thus, photoconversion is much more effective in dyad **Ru-DAE** than in the diarylethene model **DAE**. The quantum yield of the photocyclization reaction is 0.22 in air-equilibrated solution and increases to 0.44 in deaerated solution. The oxygen effect is larger here than in the diarylethene model **DAE**. Altogether, the results of the photolysis at 470 nm indicate that the light absorbed by the Ru(II) unit is very efficient in promoting the photochemical ring closure reaction of dyad **Ru-DAE**.

The photocyclization of **Ru-DAE** can be monitored also by ^{1}NMR in $CDCl_3$, following the development of the new methyl signal at 1.98 ppm characteristic of the closed form and the parallel decrease of the 2.1 and 2.3-ppm signals of the open form. The ^{1}NMR experiments confirm the photoconversion efficiency obtained by spectrophotometric analysis.

Photochemical ring opening, with complete reversal of the spectral changes of Figure 7, can be effected by irradiation of the closed form of **Ru-DAE** at $\lambda > 550$ nm CH_3CN (100% excitation of the diarylethene unit). The quantum yield is appreciably the same as that of model **DAE**, indicating

(85) In the metal complex diarylethene triads studied by De Cola,[54,55] the conformational equilibrium was completely displaced towards the antiparallel conformer. In that case, however, the points of attachment of the metal complex units were on the aromatic moieties, along the long axis of the diarylethene.

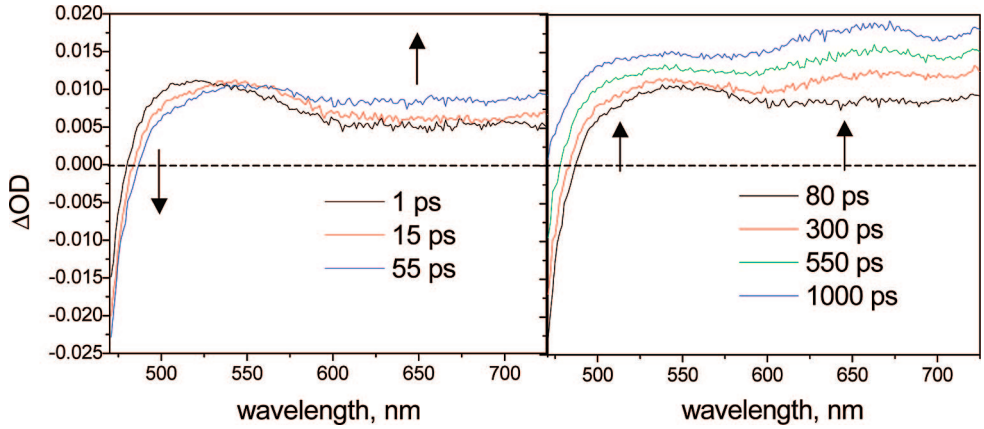

Figure 9. Transient spectra obtained by femtosecond spectroscopy of dyad **Ru-DAE** (CH_3CN, 400 nm excitation). (Left) 1−55 ps; (Right) 80−1000 ps.

negligible perturbation of the photochemistry of the diarylethene by the Ru(II) unit. On the other hand, the high yield (ca. 0.9) of closed isomer obtained at the photostationary state upon excitation in the isosbestic point at 470 nm clearly indicates that the light absorbed by the Ru(II) complex (ca. 90% at this wavelength) is highly inefficient in promoting the photochemical ring opening reaction of dyad **Ru-DAE**.

The open form of dyad **Ru-DAE** is very weakly luminescent in CH_3CN, upon excitation in the absorption maximum at 450 nm. The weak emission, with $\lambda_{max} = 600$ nm, can be assigned to MLCT phosphorescence of the Ru(II) polypyridine unit, as it is practically superimposable in terms of spectral profile to that of model system **Ru.** It is, however, much less intense than in the model, with a ratio of ca. 100 between optically matched solutions of **Ru** and **Ru-DAE**. The lifetime of this emission is below the detection limit of our apparatus (0.5 ns, see Experimental Methods). When **Ru-DAE** was excited at 400 nm, a slight distortion in the spectral profile (slight enhancement on the blue edge of the MLCT emission) was observed. This can be taken as indication of some diarylethene fluorescence (expected $\lambda_{max} = 570$) following light absorption by this molecular component (ca. 10% at 400 nm, Figure 6). However, the intensity of this fluorescence is minimal (about two orders of magnitude lower if compared to model **DAE** at equivalent absorbed light intensity). In conclusion, in the open form of dyad **Ru-DAE** both emissions, the Ru(II) MLCT phosphorescence and the diarylethene fluorescence, are strongly quenched relative to the individual molecular components. The processes responsible for this quenching can be discussed on the basis of the qualitative level diagram of Figure 8, where the excited states of the Ru(II) complex and diarylethene units are labeled Ru and DAE, respectively. The working hypothesis assumes that the diarylethene fluorescence is quenched by singlet−singlet energy transfer, whereas the Ru(II) MLCT phosphorescence is quenched by triplet−triplet energy transfer. Both processes are thermodynamically allowed, as the diarylethene singlet state is slightly higher[86,87] than that of the Ru(II) complex and $\pi-\pi^*$ states are expected to have larger singlet−triplet splittings than MLCT states (the lower energy of the diarylethene triplet is confirmed by the computational results, see below). Definite proof for these postulated quenching pathways can be obtained by the time-resolved spectroscopy results (*vide infra*).

The ultrafast spectroscopy results on **Ru-DAE** (CH_3CN, 400 nm excitation) are shown in Figure 9. In these experiments, the excitation light is absorbed ca. 75% by the metal complex and ca. 25% by the diarylethene chromophore. As a matter of

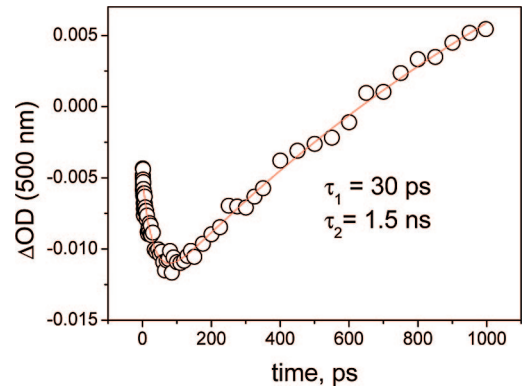

Figure 10. Kinetic analysis of the biphasic spectral changes of Figure 9.

fact, the initial spectrum (1 ps, immediately after the excitation pulse) contains spectroscopic signatures of both chromophores: (i) the bleaching of the ground-state MLCT band and the flat absorption of the reduced ligand, typical of the triplet state of the Ru(II) polypyridine chromophores; (ii) an absorption maximum at ca. 520 nm, indicative of the prompt photochemical formation of closed isomer. Two distinct types of time-resolved spectral changes are observed. In the early time scale (1−55 ps), a further development of triplet MLCT features takes place. This process can be very likely associated to the population of the triplet MLCT state of the Ru(II) complex, upon direct excitation of the diarylethene, by singlet energy transfer followed by prompt intersystem crossing. Then (at $t > 80$ ps and clearly extending into the nanosecond time scale), a disappearance of the MLCT bleaching and general increase in differential absorption takes place. By comparison with the spectra of Figures 3 and 4, these spectral changes can be assigned to the formation of diarylethene triplet as a consequence of triplet energy transfer from the Ru(II) unit.

(86) The higher energy of the DAE relative singlet excited state to the Ru(II) polypyridine one is clearly apparent from absorption spectra of Figure 6. Given the above-mentioned large Stokes shift of the DAE emission, the spectral overlap with the Ru(II) polypyridine absorption is relatively modest (Figure S1, Supporting Information). It is sufficient, however, to bring the expected energy transfer into the ps time domain. For example, using 9 Å as an average **Ru−DAE** distance and a 2/3 average orientation factor, a 50 ps time constant is predicted by the Förster equation[87] (calculations performed using PhotochemCAD; Du, H.; Fuh, R. A.; Li, J.; Corkan, A.; Lindsey, J. S. *Photochem. Photobiol.* **1998**, *68*, 141142).

(87) (a) Förster, T. *Ann. Phys.* **1948**, *2*, 55–75. (b) Förster, T. *Discuss. Faraday Soc.* **1959**, *27*, 7–17.

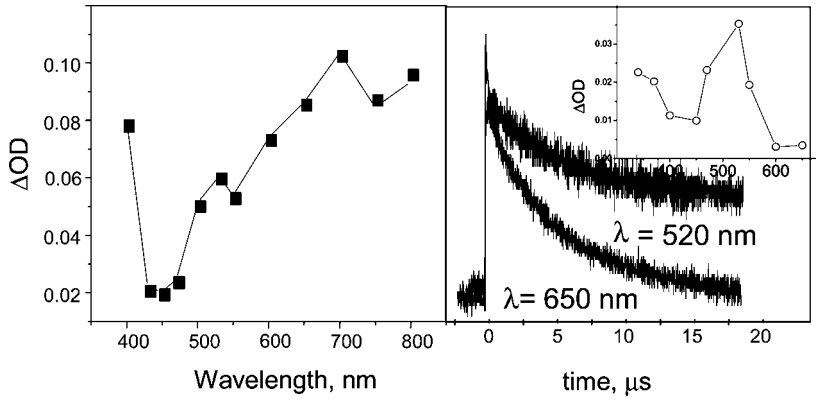

Figure 11. (Left) Transient spectrum obtained by nanosecond laser photolysis of dyad **Ru-DAE** (CH_3CN deaerated solution, 355 nm excitation, 100 ns time delay). (Right) Transient decay monitored at different wavelengths. (Inset) Spectral profile of the permanent absorption (measured at 50 μs delay).

The time constants for these two processes are 30 ps and ca. 1.5 ns, respectively (Figure 10).

In summary, the ultrafast spectroscopy of dyad **Ru-DAE** demonstrates the occurrence of two intramolecular energy transfer processes (Figure 8), namely, at the singlet level, energy transfer from the diarylethene to the complex (eq 1)

$$\mathrm{Ru(S_o)} - {}^{*}\mathrm{DAE(S_1)} \rightarrow {}^{*}\mathrm{Ru(S_1)} - \mathrm{DAE(S_o)} \qquad (1)$$

and, at the triplet level, from the Ru(II) complex to the diarylethene (eq 2)

$$^{*}\mathrm{Ru(T_1)} - \mathrm{DAE(S_o)} \rightarrow \mathrm{Ru(S_o)} - {}^{*}\mathrm{DAE(T_1)} \qquad (2)$$

Both energy transfer processes are expected to be 100% efficient, as their time constants are much shorter than the intrinsic lifetimes of the donor excited state (nanoseconds for the diarylethene, microseconds for thee Ru(II) complex). This is in line with the observed very efficient quenching of both the diarylethene fluorescence and the Ru(II) complex phosphorescence.

The fate of the triplet state of the diarylethene in dyad **Ru-DAE** can be monitored by nanosecond laser flash photolysis (Figure 11). The transient absorption spectrum (Figure 11, left) matches well that obtained with the model diarylethene (Figure 4), thus confirming the nature of the transient. It decays with an oxygen-dependent kinetics (10 and 0.40 μs in deaerated and aerated solution, respectively). The residual, permanent absorption is wavelength-dependent (Figure 11, right). It peaks at ca. 520 nm (Figure 11, inset), consistent with the spectrum of the closed isomer photoproduct. Its magnitude decreases by a factor of ca. 2 in going from deaerated to aerated solution, in agreement with the evidence recorded in continuous photochemistry.

The overall photophysical/photochemical mechanism of dyad **Ru-DAE** is summarized in Figure 8. As discussed above for the isolated diarylethene, this mechanism averages the behavior of parallel and antiparallel conformers of the dyad, which cannot be photophysically discriminated on experimental grounds.[88] Further to the data obtained on the diarylethene **DAE**, the study of dyad **Ru-DAE** provides strong evidence for a triplet path to photochemical cyclization in this class of diarylethenes. In this case, the triplet path is intramolecularly sensitized by fast Dexter energy transfer from the Ru(II) polypyridine chromophore. The computational results (see below) show that the triplet state of the open form of the diarylethene (E^{0-0}, ca. 1.7 eV) is energetically accessible from the Ru(II) polypyridine triplet (E^{0-0}, ca. 2.0 eV). Once the diarylethene triplet is populated, photocyclization takes place in the microsecond time scale. As for **DAE**, this finding is consistent with the picture obtained from the computational study (see below), where triplet photocyclization is predicted to be a slightly activated (ca. 8 kcal/mol) process. Remarkably, the conversion at photostationary state is very high in dyad **Ru-DAE** (ca. 90%) as compared with diarylethene model **DAE** (35%). As the 470-nm irradiation light is mainly (ca. 90%) absorbed by the Ru(II) polypyridine chromophore in both the open and closed forms of **Ru-DAE**, it implies that photosensitized cyclization is much more effective than cycloreversion. This cannot be due to a difference in triplet energy transfer efficiencies, as the states of the closed-ring isomer are certainly lower than those of the open-ring isomer and, indeed, the Ru(II) MLCT emission is completely quenched also in the closed form of dyad **Ru-DAE**. The reason is pointed out by the DFT calculations (see below), which show how the barrier for ring-opening along the diarylethene triplet potential energy surface is substantially higher (ca. 13 kcal/mol) than for ring-closure (ca. 8 kcal/mol).

The photophysics and photochemistry of dyad **Ru-CH_2-DAE**, differing from **Ru-DAE** in the presence of a methylene spacer between the Ru(II) polypyridine chromophore and the diarylethene unit, is qualitatively very similar to that of **Ru-DAE**. Thus, the same energy level diagram and photochemical/photophysical processes of Figure 8 apply to dyad **Ru-CH_2-DAE**. Quantitative differences are observed, however, mainly in the kinetics of the singlet and triplet intramolecular energy transfer processes. In fact, femtosecond spectroscopy shows the singlet energy transfer process with a time constant of 150 ps (as compared to 30 for **Ru-DAE**). On the other hand, the triplet energy transfer process can now be time-resolved by nanosecond flash photolysis. Figure 12 shows the initial spectrum, with typical features of the Ru(II) triplet MLCT state (bleaching at 450 nm and emission at 610 nm), evolving in time to the typical spectrum of the diarylethene triplet (positive absorption with maximum at ca. 700 nm). The time constant for this process, coincident with the lifetime of the MLCT state measured from emission, is 40 ns (to be compared with 1.5 ns for **Ru-DAE**). It is seen that insertion of a methylene spacer slows down

(88) The apparently odd result, where the lifetime of the triplet state is oxygen-quenched by a factor of 10 whereas the photocyclization quantum yield, both in stationary and pulsed experiments, is only quenched by a factor of 2, is probably related to the lack of experimental discrimination between the excited states of the parallel and antiparallel conformers.

considerably both intramolecular energy transfer processes. The difference in the magnitude of the effect for the two processes very likely reflects the difference in energy transfer mechanism,[89] Förster for the singlet−singlet process, Dexter for the triplet energy transfer process.

Comparison with Other Systems. The first demonstration of the involvement of triplet states in the photocyclization of diarylethenes was given by De Cola and co-workers[54,55] in a supramolecular system (**1**) where a photochromic dithienylperfluorocyclopentene unit was inserted as a bridge between two Ru(II) polypyridine units. Aside from the structural dissimilarities (different diarylethene units, different connection between the diarylethene and the Ru(II) chromophores), system **1** diverges from those studied in the present work in several mechanistic respects. De Cola and co-workers in their work[54,55] did not observe any long-lived transient nor any oxygen-sensitive photocyclization by direct irradiation of the free diarylethene, thus indicating a negligible intersystem crossing yield in the dithienylperfluorocyclopentene photochromic unit. Here, on the other hand, these features are observed in the diarylethene model **DAE**, indicating appreciable (ca. 30%) triplet state formation in the free bis(benzothiophene)maleimide photochromic unit. Efficient intramolecular sensitization by the Ru(II) polypyridine chromophore, with diarylethene triplet spectral features and oxygen-dependent reactivity, were observed both on **1**[54,55] and, in the present work, on **Ru-DAE** and **Ru-CH$_2$-DAE**. The energetics is somewhat different in the two types of supramolecular systems, however, as the excited-states of the dithienylperfluorocyclopentene unit are hypsochromically shifted with respect to those of bis(benzothiophene)maleimide units. Thus, the intramolecular triplet energy transfer seems to be reversible in **1**, whereas it is irreversible, from the Ru(II) polypyridine chromophore to the diarylethene, in dyads **Ru-DAE** and **Ru-CH$_2$-DAE**. The intramolecular energy transfer processes, at the singlet and triplet level, between the Ru(II) polypyridine chromophore and the diarylethene, observed in **Ru-DAE** and **Ru-CH$_2$-DAE** by femtosecond and nanosecond

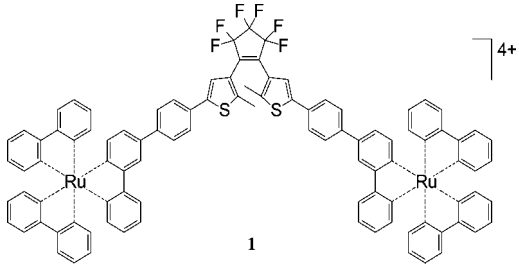

1

spectroscopy, were not time-resolved in **1**.

A related type of systems, developed by Yam and co-workers,[51–53] are Re(I) complexes of bis-thienyl substituted phenanthroline ligands **2**. These systems are not truly supramolecular, lacking a clear structural distinction between the photosensitizer and photochromic units. Nevertheless, sensitization of the photocyclization of the ligand is achieved by light absorption in the metal-to-ligand (MLCT) band. Thus, the process responsible for the photosensitization (formally analogous to the intercomponent energy transfer in **Ru-DAE**, **Ru-CH$_2$-DAE**, and **1**) is the conversion between the triplet MLCT and intraligand (IL)

(89) Turro, N. J. Ed. *Modern Molecular Photochemistry*; University Science Books: Sausalito, CA, 1991.

(90) In Figure 13, the closed-ring form is less stable by a few kcal mol^{-1}, but this order depends on the basis set used, as shown in Table 1 and Table A of the Supporting Information.

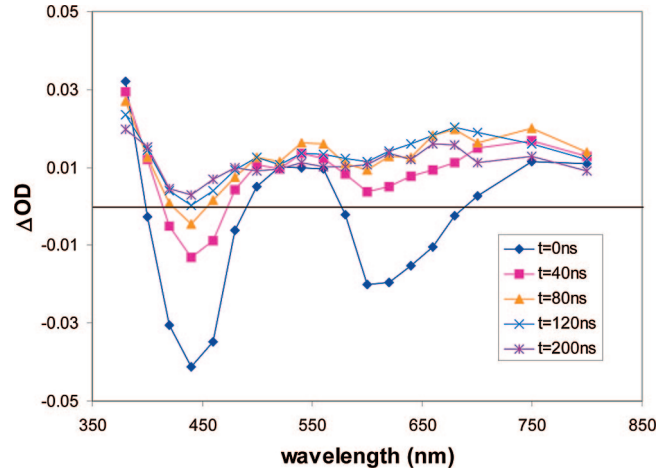

Figure 12. Transient spectral changes observed in the nanosecond laser photolysis of dyad **Ru-CH$_2$-DAE** (CH$_3$CN deaerated solution, 355 nm excitation).

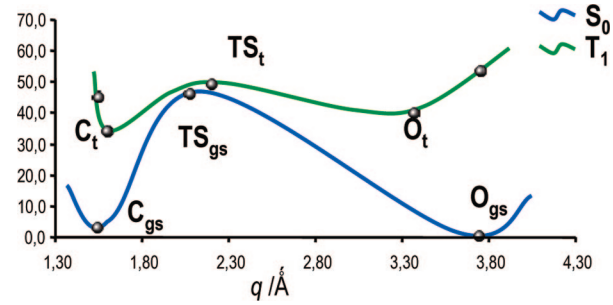

Figure 13. Outline of S_0 (blue line) and T_1 (green line) potential energy surfaces for **DAE**, from DFT calculations performed at the UB3LYP/6−31G* level. *q*, the reaction coordinate, is here simplified by the central C−C bond distance.

states, time-resolved in the ns time scale. A clear difference between **2** and the other systems seems to lie in the shorter time scale for the triplet cyclization reaction: few nanoseconds in **2**, few microseconds (decreasing to hundreds of nanoseconds upon aeration) in **1** and **Ru-DAE** or **Ru-CH$_2$-DAE**. Although several factors may determine the triplet cyclization rate (see below), this difference could likely be related to the larger spin−orbit coupling in **2**, arising from the more direct coupling

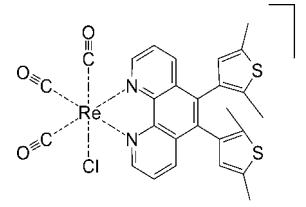

2

of the diarylethene fragment to the heavy-metal center.

Altogether, the observation of systems like **1**, **2**, and **Ru-DAE**, which irrespectively of their structural, energetic, and mechanistic differences, behave similarly in terms of sensitized photocyclization, is a clear indication that triplet reactivity should be considered as a general phenomenon in the photochemistry of diarylethenes.

Ground and Triplet State Potential Energy Surfaces. DAE. To ascertain the basic events that drive triplet photoreactivity in this class of diarylethenes, a DFT computational study has been

Table 1. UB3LYP/6-31G* Energies at the Relative Optimized Geometries for **DAE**[a]

geometry	*Q*/Å	S_0; S^2/h	ΔE (S_0)/kcal mol^{-1}	T_1; S^2/h	ΔE (T_1)/kcal mol^{-1}	ΔE (T_1-S_0)/kcal mol^{-1}
$\mathbf{O_{gs}}$	3.75	−1888.3090; 0.000 (−1887.9674)	0.0	−1888.2233; 2.001	53.8	53.8
$\mathbf{O_t}$	3.37	−1888.2873; 0.000	13.6	−1888.2451; 2.002 (−1887.9052)	40.1	26.5
$\mathbf{TS_t}$	2.23	−1888.2375; 0.470	44.9	−1888.2321; 2.001 (−1887.8917)	48.2	3.4
$\mathbf{TS_{gs}}$	2.14	−1888.2363; 0.548 (−1887.8969)	45.6	−1888.2325; 2.002	48.0	2.4
$\mathbf{C_t}$	1.59	−1888.2839; 0.000	15.8	−1888.2543; 2.006 (−1887.9127)	34.3	18.5
$\mathbf{C_{gs}}$	1.55	−1888.3039; 0.000 (−1887.9591)	3.2	−1888.2371; 2.003	45.1	41.9

[a] $\Delta E(S_0)$ and $\Delta E(T_1)$ are calculated with the open-ring S_0 minimum energy as reference. In brackets are the zero-point-energy-corrected UB3LYP/6-31G* energies. The wavefunction spin-contamination is reported along with the absolute energy values.

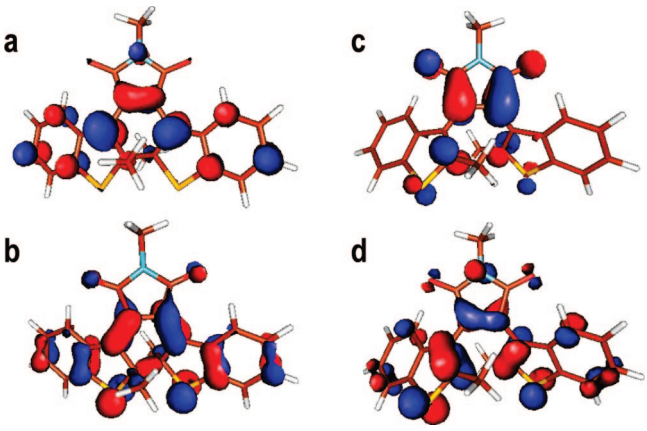

Figure 14. SOMOs isocontour plots for T_1 minima in **DAE**, at the UB3LYP/6-31G* level. (a) Highest and (b) lowest SOMO for the closed-ring isomer ($\mathbf{C_t}$); (c) Highest and (d) lowest SOMO for the open-ring isomer ($\mathbf{O_t}$).

performed on **DAE**. The calculations have focused on the investigation of ground state (S_0) and lowest triplet state (T_1) potential energy surfaces. The DFT results are summarized in Figure 13 and Table 1, whereas the optimized structures are reported in detail in the Supporting Information.

On the ground-state PES, two minima corresponding to the open- and closed-ring isomers and a transition structure connecting them (noted $\mathbf{O_{gs}}$, $\mathbf{C_{gs}}$, and $\mathbf{TS_{gs}}$, respectively, in Figure 13) have been located. The $\mathbf{O_{gs}}$ and $\mathbf{C_{gs}}$ geometries have the expected C_2 symmetry and compare well with related structures calculated for 1,2-bis(3-thienyl)ethene.[34,35,39] The reaction coordinate leading from $\mathbf{C_{gs}}$ to $\mathbf{O_{gs}}$, represented in Figure 13 by the value of the relevant C−C distance, involves a simultaneous sigma-bond breaking and a complete reorganization of the π electronic system. This reaction path, conserving the original C_2 symmetry, shows a high energy barrier (ca. 46 kcal mol^{-1}) separating the two isomers on the ground state, consistent with their experimental thermal stability. The two isomers, $\mathbf{C_{gs}}$ and $\mathbf{O_{gs}}$, have very similar energy.[90]

On T_1 PES, two C_2 minima have been located corresponding to the triplet excited-state open- and closed-ring **DAE** isomers ($\mathbf{O_t}$ and $\mathbf{C_t}$, respectively, in Figure 13). The closed-ring isomer $\mathbf{C_t}$ is definitely the most stable of the two excited-state minima. It is worth noting how the localization of the singly occupied molecular orbitals (SOMOs) drastically changes when going from the open to the closed geometry. Whereas for $\mathbf{C_t}$ the SOMOs are delocalized almost over the same atoms (Figure 14, hexatriene-based MOs a and b), for $\mathbf{O_t}$ the two SOMOs are located in different regions of the molecule, namely the hexatriene and the maleimide fragment (Figure 14, c and d). The "vertical" S_0-T_1 energy gap is calculated to be ca. 54 kcal mol^{-1} at the $\mathbf{O_{gs}}$ geometry and ca. 42 kcal mol^{-1} at the $\mathbf{C_{gs}}$ geometry. On the other hand, the 0−0 energy difference (i.e., the difference between PES minima) is 40 kcal mol^{-1} for the open-ring isomer and 31 kcal mol^{-1} for the closed-ring one. These calculated triplet state energies are relevant to the analysis of intramolecular sensitization in the **Ru-DAE** dyad (*vide infra*).

The transition state connecting $\mathbf{O_t}$ and $\mathbf{C_t}$ ($\mathbf{TS_t}$ in Figure 13), is also characterized by C_2 symmetry,[91] is located 8 kcal mol^{-1} above $\mathbf{O_t}$ and 14 kcal mol^{-1} above $\mathbf{C_t}$. Accordingly, the barrier to isomerization on the triplet state PES is much smaller than that on the ground state. In the spatial region where $\mathbf{TS_t}$ is located, the T_1 potential energy surface features a wide plateau. In the space of geometries where both $\mathbf{TS_t}$ and $\mathbf{TS_{gs}}$ sit, S_0 and T_1 surfaces turn out to be almost degenerate. Hence, there might exist a region in the space of coordinates where the two surfaces cross each other or coincide. This region should reasonably reside nearby the triplet transition state, although the IRC was not able to locate it.[92] In a later section, the proximity in energy of the two surfaces will be discussed within the framework of a two-state reactivity (TSR)[93] and the intersystem crossing (ISC) transition is related to the reaction bottleneck of the ring-closure process.

Mod-DAE. A set of assessment calculations has been performed on the prototypical system **mod-DAE** at the CASSCF// CASPT2 and DFT levels of theory to characterize S_0 and T_1 potential energy surfaces. CASSCF and DFT optimized geometries and energetics, along with CASPT2 energy corrections, are reported in detail in the Supporting Information. The essence of these results is exemplified in Figure 15.

At the CASSCF level (Figure 15 b, dashed lines), two minima corresponding to the open- and closed-ring isomers and a transition structure connecting them were located on the S_0 PES of **mod-DAE**. In Figure 15, these structures are respectively noted as $\mathbf{O_{gs}}$, $\mathbf{C_{gs}}$, and $\mathbf{TS_{gs}}$ (as to underline the analogy with **DAE**). The open-ring form is the most stable, although the energy difference between the two isomers is almost negligible. The reaction path connecting these stationary points is of C_2 symmetry and the energy barrier associated to the transition structure amounts to ca. 54 kcal mol^{-1}. The ground-state surface can be effectively compared, in terms of geometries and energy, with that of Guillaumont et al.[35] On the first triplet PES T_1, two minima on the open- and closed-ring side were found ($\mathbf{O_t}$ and $\mathbf{C_t}$ respectively), separated by a transition state ($\mathbf{TS_t}$). Also in this case the C_2 symmetry is preserved.

As far as a comparison between the theoretical methods applied to **mod-DAE** is concerned, there is a remarkable structural similarity for the transition state $\mathbf{TS_t}$ and the open-

(91) This contrasts with the asymmetric transition structure found on the first singlet excited state in a previous CASSCF study.[34]
(92) Furthermore, in a seam of S_0/T_1 surface crossings, the minimal energy crossing points (MECP) may not belong to the space described by the transition vector, and therefore, they could be reached when populating coordinates other than the reaction coordinate.
(93) Poli, R.; Harvey, J. N. *Chem. Soc. Rev.* **2003**, *32*, 1–8.

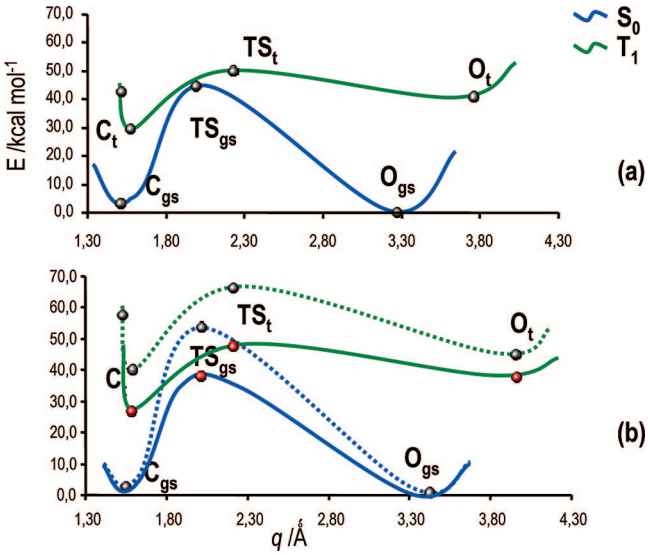

Figure 15. Outline of S_0 (blue line) and T_1 (green line) potential energy surfaces for **mod-DAE**. (a)UB3LYP/6−31G*; (b)CASSCF(10,10)/6−31G* (dashed lines) and relative CASPT2 corrections (solid lines, red markers). *q*, the reaction coordinate, is here simplified by the central C−C bond distance.

and closed-ring minima $\mathbf{O_t}$ and $\mathbf{C_t}$ optimized at the DFT and CASSCF levels of theory (see Supporting Information). In terms of energies, however, CASSCF energetics are poorer compared to DFT results, as the former does not include the dynamic correlation contribution. For this reason, the energy gap between the two surfaces of interest at the CASSCF level is typically 20 kcal mol^{-1} larger (Figure 15b). Thus, no S_0/T_1 crossings can be envisaged in the transition states region, as T_1 lies well above S_0. Moreover, the energy barrier on T_1 is much higher ($\mathbf{TS_t}$ is 22 kcal mol^{-1} above $\mathbf{O_t}$) compared to the DFT surface. Therefore, CASPT2 corrections are needed to produce reliable energy surfaces.

The excellent agreement between the CASPT2 surfaces (Figure 15b, solid lines) with the DFT set of calculations performed on **mod-DAE** at the UB3LYP/6−31G* level of theory (Figure 15a) demonstrates the two aforementioned statements. Indeed, the T_1 PES energy at the CASSCF level (Figure 15b, dashed green line) is substantially higher compared that obtained at the DFT level (Figure 15 a, green line) and the CASPT2 corrections to the CASSCF energies provide a critical improvement to the surfaces S_0 and T_1. Thus the dynamic correlation contribution is certainly of importance when considering these systems. The CASPT2 corrections are indeed responsible for lowering $\mathbf{TS_{gs}}$ energy (now only 39 kcal mol^{-1} above $\mathbf{O_{gs}}$) and T_1 PES overall. The DFT results for **mod-DAE** on S_0 show $\mathbf{TS_{gs}}$ 45 kcal mol^{-1} above the open-ring minimum. The multiconfigurational character of the latter stationary point, apparent from the CASSCF wave function where reactant and product configurations have the same weight, is not easily reproduced within a density functional scheme; thus prominent spin-contamination arises. However, the overall picture of S_0 PES is clear and the structures optimized at both levels are in very good agreement.

mod-DAE vs DAE. It is useful to compare the two molecular systems **DAE** and **mod-DAE**, at the DFT level (Figures 13 and 15, see also Supporting Information). Whereas the $\mathbf{TS_t}$ and $\mathbf{C_t}$ structures are very similar in the two systems, the structures of the open-ring minima $\mathbf{O_t}$ turn out to be somewhat different, with increased torsion around the central double bond and larger C−C distance. Two reasons may be indicated for what appears to be a discrepancy. First, **mod-DAE** has no constraints imposed on the central double bond, whereas **DAE** features a five-membered ring comprising exactly that bond. In addition, **mod-DAE** T_1 PES along the cyclization/cycloreversion reaction coordinate is described by orbitals localized just on the bis-thienylethene. With reference to **DAE**, the contribution of the maleimide fragment heavily affects the T_1 PES on the open-ring side. The switch of the SOMO character toward maleimide (depicted in Figure 14c) brings about the low-energy triplet state. Maleimide has indeed low-energy virtual orbitals, as it is an excellent electron-withdrawing group. Introduction of the maleimide fragment also reduces by a small amount, 2 and 7 kcal mol^{-1} on the open- and closed-ring side, respectively, the transition barrier on the triplet state surface (cf. Figure 13 and 15a, see also Supporting Information). Thus, the maleimide contribution affects, if only slightly, also the shape of T_1 PES.

In view of the results reported in the present paragraph, three preliminary conclusions are put forward: (i) the two levels of theory, CASSCF//CASPT2 and DFT, applied to the study of **mod-DAE** provide a congruent depiction of the system under investigation; thus, the DFT approach can reasonably be adopted when treating large systems, out of the reach of correlated *ab initio* methods; (ii) the variations to T_1 PES induced by the maleimide fragment in going from **mod-DAE** to **DAE** (topological alterations and energetic flattening on the open- and closed-ring side respectively) are of secondary importance overall; (iii) the inherent similarity between **DAE** and **mod-DAE** DFT descriptions ensures the portability of the theoretical method and uphold our conclusions (*vide infra*).

Triplet Reaction Mechanism. Cyclization. The photophysical results can be discussed with reference to the potential energy surfaces of the S_0 and T_1 states of **DAE** as a function of the reaction coordinate. Triplet photocyclization originates from the $\mathbf{O_t}$ minimum, populated by intersystem crossing from the relaxed S_1 state in the direct photochemistry of **DAE** (Figure 5) or by triplet energy transfer from the Ru(II) polypyridine unit to the diarylethene in the sensitized process of **Ru-DAE** (Figure 8).

Although the time scale for S_1-T_1 intersystem crossing (few ps) is realistic for this type of process, that for intramolecular triplet energy transfer (1.5 ns) appears to be relatively slow, considering the close proximity of the two chromophores, directly connected in the dyad by a single bond. In terms of standard theory[89,94,95] the energy transfer rate constant is given by

$$k_{en} = \frac{2\pi}{\hbar} H_{en}^2 FC \qquad (3)$$

where H_{en} is the electronic term (donor−acceptor electronic coupling for triplet energy transfer, of the exchange type) and *FC* is the nuclear term (product of Franck−Condon factors for coupled virtual transitions in donor and acceptor). From this viewpoint, two factors likely contribute to slow down in this case the energy transfer process. The large dihedral angle (ca. 70°) along the connection between the phenanthroline ligand and the maleimide group, as inferred from the calculations on the **phen-DAE** model (see Supporting Information), efficiently

(94) Orlandi, G.; Monti, S.; Barigelletti, F.; Balzani, V. *Chem. Phys.* **1980**, *52*, 313–319.
(95) Murtaza, Z.; Zipp, A. P.; Worl, L. A.; Graff, D.; Jones, W. E., Jr; Bates, W. D.; Meyer, T. J. *J. Am. Chem. Soc.* **1991**, *113*, 5113–5114.

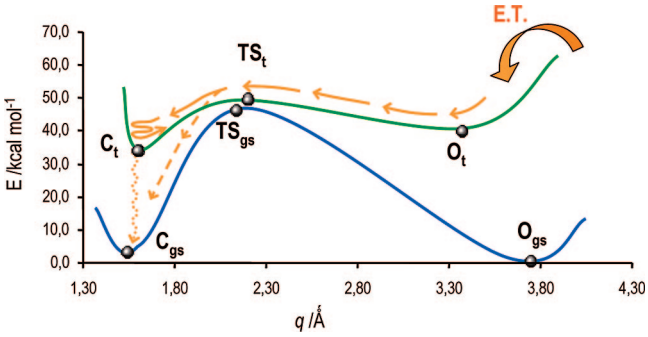

Figure 16. Schematic representation of the potential energy profiles for S_0 (blue line) and T_1 (green line) PESs calculated for **DAE**, at the UB3LYP/6-31G* level of theory. The critical structures found along the reaction coordinate q are detailed. After the energy transfer (ET) from the metallic moiety and subsequent evolution on T_1 (solid arrows), two pathways may lead to the photoproduct $\mathbf{C_{gs}}$: *nonadiabatic pathway* (dashed arrows) and *adiabatic pathway* (dotted arrows).

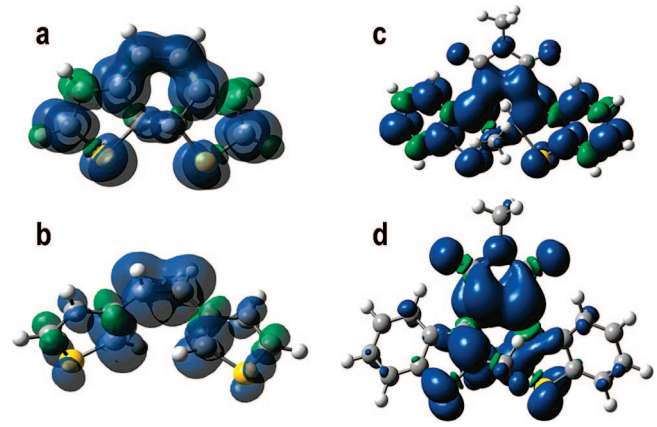

Figure 17. Spin density isocontour plots for T_1 minima at the UB3LYP/6-31G* level. Transparent surfaces for (a) $\mathbf{C_t}$ and (b) $\mathbf{O_t}$ in **mod-DAE**; solid surfaces for (c) $\mathbf{C_t}$ and (d) $\mathbf{O_t}$ in **DAE**. Blue (green) surfaces indicate excess of alpha (beta) over beta (alpha) spin electrons.

decouples the two chromophores. This implies a small exchange matrix element in the electronic term of the rate constant. Furthermore, the triplet energies in Figure 13 ("vertical" S_0-T_1 energy gap at ground-state open geometry, 54 kcal mol^{-1}, 0−0 energy difference between PES minima, 40 kcal mol^{-1}) imply that triplet energy transfer from the ^{3}MLCT state of the Ru polypyridine moiety (0−0 energy, ca. 50 kcal mol^{-1} [96]) may be energetically allowed in **Ru-DAE** only as a "non-vertical"[97,98] process leading to the $\mathbf{O_t}$ minimum as discussed above. This implies relatively small Franck−Condon factors in the nuclear term of the energy transfer rate constant (eq 3).

Once reached, the $\mathbf{O_t}$ minimum of the diarylethene T_1 state is relatively shallow and thermal energy will allow the excited species to evolve along the minimum-energy path toward the transition state region and eventually to products (Figure 16). The lifetime of the T_1 state is expected to depend on the barrier encountered along this path, calculated in this work as ca. 8 kcal mol^{-1}. Using the Eyring equation,[99]

$$k = \frac{k_B T}{h} e^{\frac{\Delta S^{\neq}}{R}} e^{-\frac{\Delta H^{\neq}}{RT}} \qquad (4)$$

the barrier height calculated in this work would yield a rate constant of about $4 \cdot 10^6$ s^{-1} (i.e., a triplet lifetime of ca. 0.3 μs) at room temperature, assuming that $\Delta S^{\neq} = 0$. For a cyclization reaction, however, the actual activation entropy is likely to be negative, as internal rotational degrees of freedom in the reactant are converted into vibrations in the product.[100] Thus, the actual lifetime of the triplet state, ca. 10 μs, is fully compatible with the calculated barrier to cyclization.

From $\mathbf{TS_t}$, the system may reach the ground-state closed-ring product ($\mathbf{C_{gs}}$) following two distinct pathways. In the case of a *nonadiabatic pathway*, a S_0/T_1 crossing funnel is accessed after passing the energy barrier on T_1, the final step of the process being an intersystem crossing, followed by fast thermalization of the vibrational motion of the system in the minimum $\mathbf{C_{gs}}$ on S_0 (Figure 16, dashed arrows). In the case of an *adiabatic pathway*, after crossing the barrier the system reaches the excited-state minimum $\mathbf{C_t}$, the final step of the process being a radiationless decay from minimum $\mathbf{C_t}$ to $\mathbf{C_{gs}}$ (Figure 16, dotted arrows). An additional possibility for deactivation from **Ct** is to revert, via an activated process, to the S_0/T_1 crossing seam and follow the final step of the nonadiabatic pathway.

According to standard models,[101] the $T_1 \rightarrow S_0$ ISC rate depends on spin−orbit coupling (SOC) matrix element between the two electronic wave functions and on ground-state density of rovibronic states at energy comparable to T_1. Therefore, additional calculations have been performed on **mod-DAE** at the CASSCF(8,8)/6-31G* level,[102] to evaluate S_0/T_1 SOC. The results indicate that the spin−orbit coupling between the two surfaces of interest is highly dependent on geometry. At $\mathbf{C_t}$ minimum the SOC has a value of 8.3 cm^{-1}, whereas at $\mathbf{O_t}$ minimum it is lowered to 1.5 cm^{-1}. ISC is likely to take place in the transition-state region, where T_1 and S_0 PES are almost degenerate, the Franck−Condon factors and the ground-state density of states are more favorable than at open- or close-ring geometries. Assuming that the geometric divide for spin−orbit coupling (*SOC-divide*) is located at $\mathbf{TS_t}$ geometry, the above calculations suggest that the most effective region (in terms of S_0/T_1 crossing seam) for ISC is likely situated on the closed-ring isomer side of $\mathbf{TS_t}$. The aforementioned reasons allow the indication of the *nonadiabatic pathway* as the most probable process.

Some caution must be taken in extrapolating these SOC arguments from **mod-DAE** to **DAE** and **Ru-DAE**. First, **mod-DAE** lacks the maleimide fragment and the reduction of the active space[102] may unbalance the description of the electronic states. Nevertheless, SOC change depends on the spin density delocalization[103] and the change of spin density contour along the reaction coordinate is a common feature of **DAE** and **mod-DAE** (Figure 17). Therefore, the geometric divide for spin−orbit

(96) Juris, A.; Balzani, V.; Barigelletti, F.; Campagna, S.; Belser, P.; von Zelewsky, A. *Coord. Chem. Rev.* **1998**, *84*, 85–277.
(97) Scandola, F.; Balzani, V. *J. Chem. Educ.* **1983**, *60*, 814–823.
(98) Balzani, V.; Bolletta, F.; Scandola, F. *J. Am. Chem. Soc.* **1980**, *102*, 2152–2163.
(99) Laidler, K. J. Theories of Reaction Rates. In *Chemical Kinetics*; Harper & Row: New York, 1987; Chapter 4.
(100) Frost, A. A.; Pearson, R. G. *Kinetics and Mechanism*; John Wiley & Sons, Inc.: New York, 1961.
(101) Harvey, J. N.; Grimme, S.; Woeller, M.; Peverimhoff, S. D.; Danovich, D.; Shaik, S. *Chem. Phys. Lett.* **2000**, *322*, 358–362, and references therein.
(102) The reduced active space is due to the algorithm used, which requires full diagonalization of the CI matrix.
(103) Harvey, J. N.; Aschi, M. *Phys. Chem. Chem. Phys.* **1999**, *1*, 5555–5563.

coupling is likely to be located at $\mathbf{TS_t}$ geometry in both systems. A second aspect to be considered is that the presence of the metal atom in **Ru-DAE** might be liable for enhancing spin−orbit coupling. On the basis of the Breit-Pauli formalism, where SOC depends on the inverse third power of the distance from the heavy atom,[104] with a minimum distance of ca. 9 Å between the two moieties in **Ru-DAE** the heavy-metal effect is expected to be negligible.

Cycloreversion. The experimental results clearly show that light absorbed by the Ru moiety is inefficient in promoting the photochemical ring-opening reaction of dyad **Ru-DAE**. The population of the T_1 state of the diarylethene closed-ring isomer from the ^{3}MLCT state of the Ru moiety is energetically allowed ("vertical" S_0-T_1 energy gap at the $\mathbf{C_{gs}}$ geometry, ca. 42 kcal mol^{-1}) and efficient, as witnessed by the efficient quenching of the Ru-based emission. Hence, the reason must originate from inefficient cycloreversion within the diarylethene T_1 state. In fact, $\mathbf{C_t}$ is a relatively deep minimum along the T_1 surface, with a 13 kcal mol^{-1} energy barrier to $\mathbf{TS_t}$ along the MEP. An activated process leading to the transition-state region is expected to be quite slow (ca. 0.6 ms) and would probably compete inefficiently with the radiationless decay (by nuclear tunneling) of $\mathbf{C_t}$ to the ground state. Moreover, even if thermal activation to the transition-state region could be achieved, ISC would probably lead back to the closed-ring ground-state minimum $\mathbf{C_{gs}}$, as the most efficient S_0/T_1 crossing likely sits on the closed-ring isomer side of $\mathbf{TS_t}$ (see discussion above). In conclusion, the experimental lack of sensitized cycloreversion is easily accounted for in terms of barrier height and SOC arguments.

Conclusions

This investigation has provided clear experimental evidence for the participation of triplet state in the photochromic behavior of this class of diarylethenes. Unlike previous studies,[51–55] evidence for triplet reactivity case is obtained here not only for the metal-containing systems but also for the isolated diarylethene **DAE**, where, besides prompt reaction from the singlet state, an additional oxygen-sensitive triplet channel for photocyclization is detected. The triplet pathway becomes more efficient in the dyads (**Ru-DAE** and **Ru-CH$_2$-DAE**), because of predominant light absorption and efficient sensitization by the Ru(II) polypyridine unit. A complete kinetic characterization of the dyads has been obtained. Besides prompt photocyclization (0.5 ps), fast singlet energy transfer takes place from the directly excited diarylethene to the Ru(II) chromophore (30 ps in **Ru-DAE**, 150 ps in **Ru-CH$_2$-DAE**). In the Ru(II) chromophore, ultrafast intersystem crossing to the MLCT triplet state is followed by triplet energy transfer to the diarylethene (1.5 ns in **Ru-DAE**, 40 ns in **Ru-CH$_2$-DAE**). The triplet state of the diarylethene undergoes cyclization in a microsecond time scale.

The computational study provides a working model for the triplet reactivity of this class of photochromic diarylethenes. The DFT results on **DAE** outline the following key features for the potential energy surfaces of the ground state (S_0) and first triplet state (T_1): (i) on S_0, a large isomerization barrier (ca. 45 kcal mol^{-1}) separates the two minima, whereas on T_1 the activation barrier for the same process is much lower; (ii) on T_1, the barrier for cycloreversion (ca. 14 kcal mol^{-1}) is definitely larger than that for cyclization (ca. 8 kcal mol^{-1}); (iii) the transition-state structures on S_0 and T_1 are similar and lean, along the reaction coordinate, toward the closed-ring isomer; (iv) at the transition-state geometry, the ground-state and triplet PES are almost degenerate. These features allow a detailed rationalization of the photoreactivity observed for **Ru-DAE**, where the triplet state of the diarylethene is efficiently populated by energy transfer from the ruthenium-polypyridine sensitizer unit. When the open-ring minimum on T_1 is populated, activation to the transition state is relatively undemanding (8 kcal mol^{-1}) and takes place in the few microsecond time scale. In the transition-state region, fast ISC takes place at a S_0/T_1 crossing funnel, presumably displaced toward the closed-ring isomer, where more favorable SOC occurs. Next, relaxation along the ground-state PES leads efficiently to the cyclized product. An adiabatic process, where the ring-closure reaction is accomplished entirely on the triplet-state PES followed by radiationless deactivation of the triplet closed-ring form, is an alternative pathway though less likely to take place. On the other hand, when the closed-ring minimum on T_1 is populated by energy transfer from the sensitizer, cycloreversion is inefficient because of the larger activation energy (slow process, expected in the ms time scale) and due to the larger SOC in the closed-ring region (inefficient process, early ISC leading back to the closed-ring minimum on S_0).

Interestingly, the main topological features of the ground- and triplet-state PES of **DAE** are reproduced (at the *ab initio* CASPT2 and DFT level) on the smaller system **mod-DAE** containing the very essential components of this class of photochromic molecules. This suggests that the above mechanistic features are not limited to diarylethenes of the maleimide type, but are probably common to many other diarylethenes. As a matter of fact, similar type of behavior (efficient photosensitized cyclization, inefficient photosensitized cycloreversion) seems to be a common feature in triplet sensitized photochromism of other types of diarylethenes.[51–55]

Acknowledgment. We are grateful to Valeria Dissette for experimental assistance and to Piero Altoè for fruitful discussions. Financial support from MUR (PRIN 2006030320 and FIRB RBNE019H9K) is gratefully acknowledged.

Supporting Information Available: Syntheses and characterization (^{1}H NMR, FT-IR, ESI) of all the compounds; emission spectrum of **DAE**; DFT structure and frontier orbitals of **phen-DAE**; DFT structures and energies of **DAE**; CASSCF, CASPT2, and DFT structures and energies of **mod-DAE**; Cartesian coordinates of the optimized structures; complete authors list of ref 80 and 81. This material is available free of charge via the Internet at http://pubs.acs.org.

JA711173Z

(104) Abegg, P. W.; Ha, T.-K. *Mol. Phys.* **1974**, *27*, 763–767, ref 254 G03-SOC in CASSCF